Journal of Catalysis 300 (2013) 30–36

Contents lists available at SciVerse ScienceDirect

Journal of Catalysis

journal homepage: www.elsevier.com/locate/jcat

Structural and surface study of calcium glyceroxide, an active phase for biodiesel production under heterogeneous catalysis

Laura León-Reina [a], Aurelio Cabeza [b,*], Jordi Rius [c], Pedro Maireles-Torres [b], Ana C. Alba-Rubio [d], Manuel López Granados [d,*]

[a] Servicios Centrales de Apoyo a la Investigación, SCAI, Universidad de Málaga, Campus Teatinos s/n. 29071-Málaga, Spain
[b] Departamento de Química Inorgánica, Cristalografía y Mineralogía (Unidad Asociada al ICP-CSIC), Universidad de Málaga, Campus Teatinos s/n. 29071-Málaga, Spain
[c] Institut de Ciència de Materials de Barcelona, 08193 Bellaterra, Catalunya, Spain
[d] Instituto de Catálisis y Petroleoquímica (CSIC), C/ Marie Curie 2, Campus de Cantoblanco, 28049-Madrid, Spain

ARTICLE INFO

Article history:
Received 23 October 2012
Revised 13 December 2012
Accepted 14 December 2012

Keywords:
Calcium glyceroxide
Biodiesel
Heterogeneous catalysis

ABSTRACT

Calcium diglyceroxide has been reported as a very active phase in the transesterification of triglycerides with methanol for biodiesel production. This work reports on the determination of the crystal structure of Ca diglyceroxide by Patterson-based direct methods from synchrotron X-ray powder diffraction (XRD) data in combination with characterisation by Differential Thermal Analysis-Thermogravimetry (DTA-TG), Scanning Electron Microscopy (SEM) and X-ray Photoelectron and Fourier Transform-Infrared spectroscopies (XPS and FT-IR). Its crystal structure is formed by molecular tetramers held together by a complex H-bond network. Both the XRD structural determination and the O1s XPS core level indicate the presence of a basic non-protonated O^- anion at the surface of Ca diglyceroxide. Along with the presence of surface lipophilic CH_x units, this O^- anion may be the origin of this molecule's high activity relative to CaO.

1. Introduction

The synthesis of a calcium glyceroxide was first reported by Grün and Bockish [1], who obtained the triglyceroxide phase, whereas Wheeler in 1931 described the preparation of calcium mono- and diglyceroxides by heating calcium oxide with excess glycerol at 60 and 110 °C, respectively [2], demonstrating that these two glyceroxides can be interconverted at a suitable temperature. Later, Fujii and Kondo undertook the study of the CaO-glycerol system from approximately 10 to 150 °C, aiming to clarify the identity of the different calcium glyceroxide phases and their thermal stabilities [3]. Additionally, calcium glyceroxide has been demonstrated to be an active phase in the transesterification of triglycerides of vegetable oils with low-molecular-weight alcohols (methanol and ethanol) to produce biodiesel.

Calcium oxide (CaO) is one of the most promising solid basic catalysts for the production of biodiesel [4–7]. At the beginning of the transesterification, calcium oxide is the active phase. However, once glycerol is produced as a by-product of the reaction, it reacts with CaO producing, calcium diglyceroxide (CaD):

$$CaO + 2C_3H_8O_3 \rightarrow Ca(C_3H_7O_3)2 + H_2O.$$

Kouzu et al. [8,9] verified that this compound is the active phase of the collected catalyst rather than other unknown calcium compounds present as minor constituents. CaD prepared as a reference sample was proven to be as active as the catalyst recovered after the transesterification process. They found that glycerol was more reactive with CaO than methanol, as the immersion of CaO in methanol reflux in the presence of glycerol only produced CaD. To facilitate the handling of the solid base catalyst, Kouzu et al. recommended the previous conversion of CaO into CaD by immersion in a methanol solution of glycerol [8].

Further support of the hypothesis that CaD is the active phase comes from the work of López Granados et al. [10], who demonstrated that the activity of Ca oxide can be increased by creating Ca glyceroxide sites at the surface of Ca oxide. Different synthetic strategies were used to create progressively higher numbers of Ca glyceroxide surface sites by the utilisation of increasingly large amounts of either diglycerides or monoglycerides or glycerol. A relationship between the prevalence of Ca glyceroxide surface sites and the improvement of the reaction rate was observed. Beyond a certain point, no improvement was achieved, indicating that the surface becomes fully covered by Ca glyceroxide species.

Despite the importance of CaD as the active phase for biodiesel production in the presence of CaO and although the synthesis of calcium glyceroxides has been known since 1910 [1], to our knowledge, no structural information about these compounds has been published. The purpose of this paper is to present a detailed study

* Corresponding authors.
E-mail addresses: aurelio@uma.es (A. Cabeza), mlgranados@icp.csic.es (M. López Granados).

0021-9517/$ - see front matter © 2012 Elsevier Inc. All rights reserved.
http://dx.doi.org/10.1016/j.jcat.2012.12.016

of the CaD crystal structure to provide a possible explanation of its outstanding catalytic activity. For this purpose, synchrotron X-ray powder diffraction data have been collected to solve its crystal structure following an *ab initio* procedure. The use of this high-resolution radiation has been essential to its determination due to the complexity of the structure, with a unit cell volume close to 4000 $Å^3$ and light atoms as main components.

2. Experimental section

2.1. Synthesis of calcium diglyceroxide

Fresh CaO was obtained by the calcination of $CaCO_3$ (Sigma–Aldrich, >99.5%) under dry air at 800 °C for 2 h (heating rate 10 °C min^{-1}) in a quartz reactor. Next, 500 mg of this fresh CaO was poured directly into a flask containing 100 mL of MeOH and 35 mL of glycerol. To avoid exposure to ambient air in this step, the flask had been previously flushed with a N_2 flow to remove the ambient air therein and the CaO was directly incorporated from the reactor in which $CaCO_3$ had been calcined. These precautions were taken to prevent the carbonation and hydration of the fresh CaO with the CO_2 and H_2O present in ambient air. Once CaO was poured over the methanol–glycerol mixture, the flask was hermetically closed to prevent contact with ambient air. Next, this mixture was heated at 50 °C and left under agitation overnight. Initially, the CaO solid dissolved slowly into the mixture. After few minutes, some turbidity was visible and a pale yellow solid gradually became apparent and more concentrated. This solid was recovered by filtration and washed twice with methanol. The solid was stored under nitrogen to prevent extensive carbonation and hydration.

2.2. Transesterification of sunflower oil with methanol

The catalytic performance of the solid prepared (CaD) was evaluated in the methanolysis of sunflower oil. The recovered solid was added to a 500 mL bolted closure autoclave reactor from Autoclave Engineers (with a magnet-driven agitator and a thermostatically controlled heating jacket) containing 135 mL of methanol (Scharlau, Reag. Ph. Eur. >99.8% GC, H_2O < 0.005%). Considering that approximately 1 mg CaO_{eq} mL^{-1} is solubilised in mixtures methanol–glycerol at 60 °C [11] and that we started from 500 mg of CaO, it can be estimated that the reaction was performed with approximately 0.7 wt.% catalyst (referenced to the oil mass employed). The reaction started when 220 mL of sunflower oil (methanol/oil molar ratio of 14) preheated at 60 °C was added to the methanol and catalyst mixture under vigorous agitation (1000 rpm). The reaction was conducted at 60 °C under autogenous pressure.

The catalytic behaviour of CaD was compared with that of CaO. To this end, 500 mg of fresh CaO (obtained by the calcination of $CaCO_3$) (0.23 wt.% of catalyst referred to the oil mass) was tested in the methanolysis of sunflower oil following the procedure described above.

Aliquots for sampling analysis were neutralised with a slight excess of 0.1 M HCl to stop the reaction, and the resulting solution was washed with dichloromethane. This washing step with HCl and dichloromethane was performed twice. The alcohol phase (water, glycerol, methanol, HCl, and $CaCl_2$) was separated from the ester phase (glycerides, dichloromethane, and methyl esters) by decantation, and the residual dichloromethane in the methyl esters phase was removed by evaporation at 80 °C. Once the methyl esters were purified, quantitative analysis was carried out following a procedure described elsewhere [4]. Briefly, the fatty acid methyl esters (FAMEs) content was determined in accordance with the European regulated procedure EN 14103 using a gas chromatograph (Agilent 6890GC) connected to a flame ionisation detector (FID) equipped with an HP INNOwax capillary column.

2.3. Characterisation techniques

Elemental analyses (C, H, N) were conducted using a Perkin–Elmer 240 analyser. Thermogravimetric and Differential Thermal Analysis (TGA and DTA) data were recorded on a SDT-Q600 analyser from TA instruments. The temperature was varied from room temperature to 1000 °C at a heating rate of 10 °C min^{-1}. The measurements were carried out on a sample in an open platinum crucible under air flow. Scanning electron micrographs (SEM) were obtained using a JEOL SM 840. The sample was placed over an aluminium drum and covered with a gold film using a JEOL Ion Sputter JFC 1100.

X-ray photoelectron spectroscopy (XPS) studies were performed with a Physical Electronics PHI 5700 spectrometer equipped with a hemispherical electron analyser (model 80-365B) and a Mg Kα (1253.6 eV) X-ray source. High-resolution spectra were recorded at a 45° take-off angle by a concentric hemispherical analyser operating in the constant pass energy mode at 29.35 eV using a 720-mm-diameter analysis area. Charge referencing was performed against adventitious carbon (C 1s 284.8 eV). The pressure in the analysis chamber was kept below $5{\cdot}10^{-6}$ Pa. PHI ACCESS ESCA-V6.0 F software was used for the data acquisition and analysis. A Shirley-type background was subtracted from the signals. The recorded spectra were always fitted using Gauss–Lorentz curves to accurately determine the binding energy of the different element core levels.

The Fourier transform infrared (FTIR) spectra were recorded at room temperature at a resolution of 4 cm^{-1} with a Nicolet 5700 Fourier transform spectrophotometer equipped with an Hg–Cd–Te cryodetector working in the range of 4000–650 cm^{-1}. For the glycerol spectrum, KBr was impregnated with glycerol and the mixture was loaded into the cup of a DRIFT accessory. The DRIFT spectrum was taken as the spectrum of glycerol. Further details are given in Ref. [10]. In the case of CaD, it was mixed with KBr and used to make a self-supported wafer. In this case, the IR spectrum of the wafer was recorded in transmittance mode.

A high-resolution powder pattern of CaD was collected on the ESRF ID31 powder diffractometer (Grenoble, France) (λ = 0.2998 Å). The Debye–Scherrer configuration was used, with the sample loaded in a rotating borosilicate glass capillary of 1.0 mm diameter. The overall measuring time was selected as ≈100 min to obtain good statistics over the angular range of 2.3–17° (in 2θ). The data from the multianalyser Si(1 1 1) stage were normalised and binned into 0.003° step sizes using local software.

3. Results and discussion

3.1. Catalytic behaviour

The catalytic performance of the prepared solid was tested in the methanolysis of sunflower oil. Its activity was compared with that obtained by the same amount of CaO (500 mg) used for preparing the CaD. Fig. 1 displays the kinetics of the reaction with both catalysts. The prepared solid was much more active than CaO, achieving a biodiesel yield above 80 wt.% after 2 h of time-on-stream, whereas that for CaO was ca. 20%. After 5 h, the FAME yields of both solids were close to the equilibrium value, which was reached asymptotically. The curve representing CaO is sigmoid, which indicates an induction period during the reaction: the reaction rate is quite small initially, but after ca. 90 min, the rate increases remarkably. As the reaction progresses and glycerol

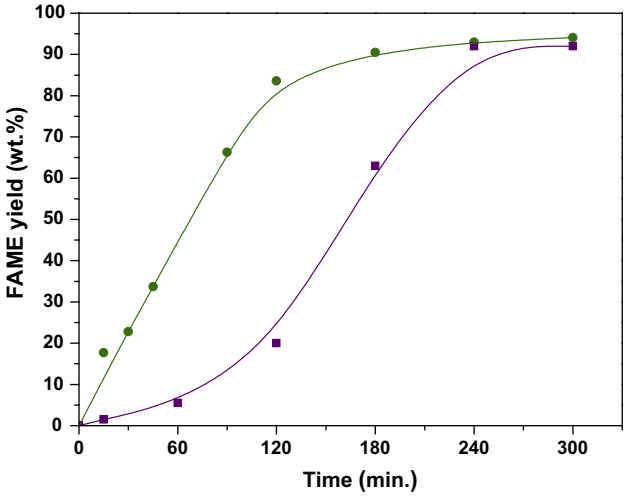

Fig. 1. Kinetics of the methanolysis of sunflower oil with (●) Ca diglyceroxide (0.7 wt.% referred to the oil mass) and (■) CaO (0.2 wt.% referred to the oil mass) (methanol/oil molar ratio = 14, 60 °C, autogenous pressure, 1000 rpm).

is formed, CaO is transformed into the more active diglyceroxide, after which the rate increases. However, when using CaD, the induction period is eliminated. These data agree well with those reported elsewhere [9,10].

3.2. General characterisation

Fig. 2 shows an SEM image of the $Ca(C_3H_7O_3)_2$ particles with sizes ranging between 1 and 5 μm exhibiting the typical tablet shape of CaD. The thermal evolution of these particles includes two weight losses, as shown in Fig. 3. The first mass loss takes place with a strong exothermic effect between 160 and 425 °C and corresponds to the decomposition of the glyceroxide anions to give calcite. The observed mass loss, 54.7%, is in good agreement with the calculated one, 55.0%. The second weight loss, between 650 and 800 °C, is attributed to the decarbonation process to give CaO. The total weight loss corresponding to decomposition and decarbonation is 73.1%, in agreement with the calculated 74.8%. The formation of CaD was further confirmed by chemical analysis, which gave a carbon content of 31.4% and a hydrogen content of 6.2% H, which are very close to the values expected from stoichiometry (32.4% and 6.3%, respectively).

The IR spectra of glycerol and CaD are presented in Fig. 4, and the main bands are summarised in Table 1 The DRIFT spectrum

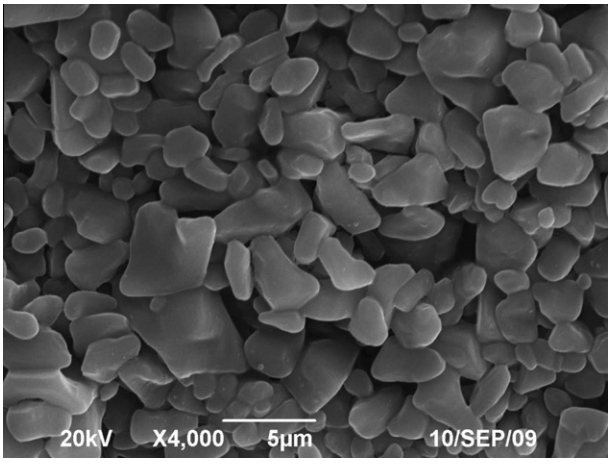

Fig. 2. SEM micrograph of calcium diglyceroxide.

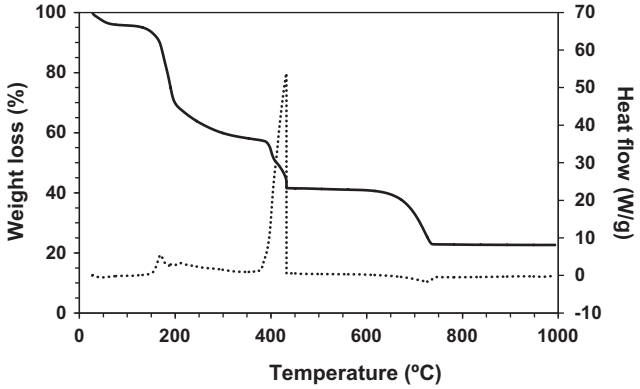

Fig. 3. Thermogravimetric Analysis (TGA) and Differential Thermal Analysis (DTA) of calcium diglyceroxide.

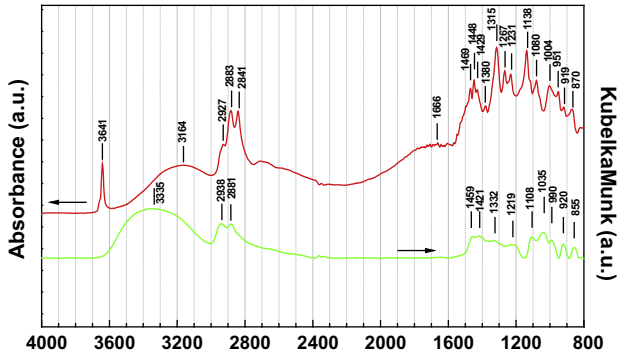

Fig. 4. IR spectra of glycerol (below) and calcium diglyceroxide (above).

Table 1
Assignment and wavenumbers (cm^{-1}) of the main IR bands for glycerol in DRIFT mode and for Ca diglyceroxide in transmittance mode.

Compound	Glycerol	Ca glyceroxide
ν_{O-H} in C–O–H	3335	3641
ν (C–H)	2938, 2881	2927, 2883, 2841
(C–H), (C–O–H) bending modes	1459, 1421, 1332, 1219, 990, 920	1469, 1448, 1429, 1380, 1315, 1267, 1231, 1004, 951, 919
ν (C–O)	1108, 1035	1138, 1080
ν (C–C)	855	870

of glycerol shows the following characteristic bands: 3335 cm^{-1}, assigned to the O–H stretching vibrations from H-bonded liquid glycerol molecules; 2938 and 2881 cm^{-1}, assigned to C–H stretching vibrations; and 1108 and 1035 cm^{-1}, assigned to the C–O stretching vibration of secondary and terminal alcohol groups. Finally, the C–O–H bending modes are observed between 1460 and 850 cm^{-1}. A more detailed discussion on the latter assignments is given elsewhere [12–15].

The IR spectrum of solid CaD is quite different from that of glycerol (Fig. 4). The shift in the band positions and the superior band resolution are clear indicators of the formation of highly crystalline CaD. These changes in the position of the bands with respect to those observed in pure alcohol have also been reported in other alkoxides, such as Na methoxide, Na ethoxide and Na propoxide [16], although some new bands may also arise from new neighbourhoods. Thus, the band at 3641 cm^{-1}, absent in the glycerol spectrum, can be attributed to the OH stretching vibration of the C–OH groups of glyceroxide units bonded to the calcium atoms. The bands at 2927, 2833, and 2841 cm^{-1} are associated with the

C–H stretching vibration and are slightly shifted with respect to pure glycerol. A similar situation was observed for the bands assigned to the various bending modes of C–H bonds (1469, 1448, 1429, 1267, 1231, 1004, 951, and 919 cm^{-1}), C–O–H bending modes (1380 and 1315 cm^{-1}), and the stretching mode of C–O bonds (1138 and 1080 cm^{-1}) of glyceroxide units. However, the possible contribution of water physisorbed on the surface of the solid cannot be discarded, based on the broad bands observed at 3164 and 1666 cm^{-1}.

3.3. Structural and surface studies

The synchrotron X-ray diffraction powder pattern of CaD was indexed with DICVOL06 [17], and integral systematic extinctions confirmed an *F*-centred orthorhombic space group. No additional systematic extinctions were observed. The integrated intensities were extracted with DAjust [18] and introduced in the Patterson-function direct-methods program XLENS [19] assuming the non-centrosymmetric space group *F222* (#22). The number of large and weak *E* values actively used was 154 and 471, respectively. The best XLENS solution showed all the atomic positions except those of three carbon atoms of one glyceroxide group, which were localised on a difference Fourier map. The final model was obtained by restrained Rietveld refinements [20] with GSAS [21,22]. The soft constrains applied to the glyceroxide groups were C–C [1.50(1) Å] and C–OH [1.40(1) Å], and the final weight was 15. No attempts to locate the H atoms were carried out due to the limited quality of the powder data. A common atomic displacement parameter for each atomic type was refined. Final Rietveld residuals were $R_{wp} = 0.080$, $R_P = 0.063$, and $R_F = 0.065$ for 563 reflections, 7349 data points, 18 restraints, and 75 refined parameters. Other crystallographic data for $Ca(C_3H_7O_3)_2$ are as follows: $a = 21.3356(1)$ Å, $b = 13.53610(9)$ Å, $c = 13.35806(8)$ Å, $V = 3857.82(6)$ $Å^3$, 16 chemical formulas per unit cell (Z), and $\rho_{calc} = 1.433$ g cm^{-3}. The final Rietveld plot is shown in Fig. 5. The crystal structure information has been deposited at the CCDC with the reference code #828033.

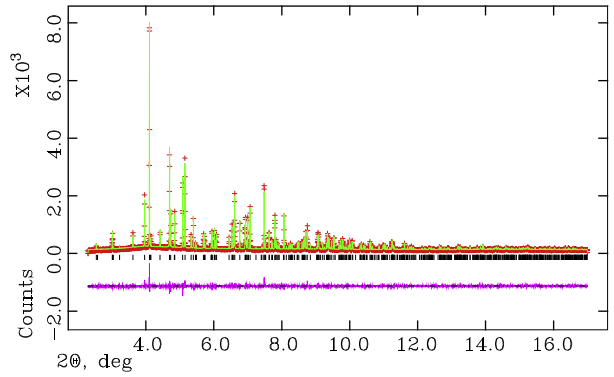

Fig. 5. Observed (crosses), calculated (solid line), and difference plots for the final Rietveld refinement of calcium diglyceroxide, $Ca(C_3H_7O_3)_2$. The vertical bars highlight permitted Bragg peak positions.

The X-ray diffraction study shows that the crystal structure of CaD may be described as a set of molecular calcium tetramers interlinked through a singular H-bond network. The point group symmetry of each isolated $Ca_4(C_3H_7O_3)_8$ tetramer is *222* (Fig. 6A). Neighbouring tetramers are related by *F* lattice symmetry operations; consequently, there are four tetramers in the unit cell according to the *F222* space group symmetry (Fig. 6B). Inside each tetrameric unit, Ca^{2+} ions form tetrahedral clusters. As seen in Fig. 6A, the coordination polyhedron of Ca^{2+} is a pentagonal bipyramid with Ca–O bond distances ranging from 2.370(6) to 2.579(5) Å (Table 2). Each tetramer contains two types of symmetry-independent glyceroxide anions. One type is the chelation of a single Ca^{2+} ion through the O1 and O2 oxygen atoms. The remaining oxygen atom (O3) of glyceroxide points towards the outside of the tetramer (see Fig. 6). The second type of glyceroxide anion comprises one oxygen atom (O5) bound to three Ca^{2+} atoms of a unique cluster; however, the two remaining oxygen atoms (O4 and O6) are each bound to only one Ca^{2+}. The existence of tetramers in CaD strongly suggests that the simplest calcium repeat unit found in CaO (a tetrahedron with Ca ions at the vertices) is preserved during the CaD synthesis by replacing the O^{2-} ligands by the O^- ions of glyceroxide.

According to the XPS results (Fig. 7), the Ca 2p region exhibits two symmetric bands at 346.8 and 350.3 eV corresponding to the typical doublet, Ca $2p_{3/2}$ and Ca $2p_{1/2}$ components, with a separation of 3.5 eV. The Ca $2p_{3/2}$ value appears at lower binding energies than those assigned to CaO/calcite (347.1–347.7 eV) [23,24], thus

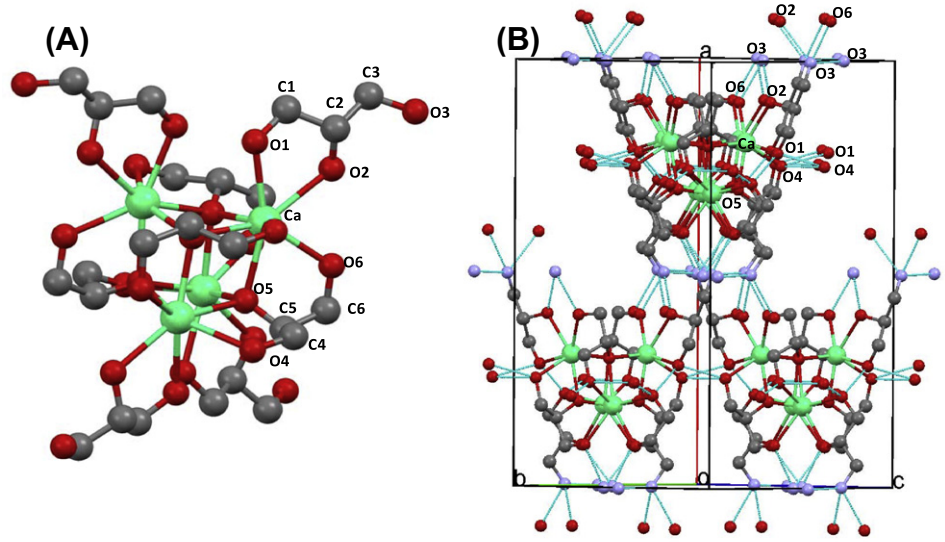

Fig. 6. (A) Molecular structure of the $Ca(C_3H_7O_3)_2$ tetramer with atoms labelled. (B) View of the packing in the unit cell with expanded contacts to better visualise the H bonds (in cyan), with O3 atoms in blue. (For interpretation of the references to colour in this figure legend, the reader is referred to the web version of this article.)

Table 2
Selected bond distances (Å) and balance of bond valences (lower values in *vu*) for $Ca(C_3H_7O_3)_2$.

Atom	Ca	(H1)	(H2)	(H3)	(H4)	(H6)	$\Sigma_C\ v^a$
O1	2.506(5)						
	0.26	0.50 (2×)			0.21		0.97
O2	2.579(5)						
	0.22		0.75				0.97
O3	–						
			0.25	0.50 (2×)		0.26	1.01
O4	2.510(7)						
	0.26				0.79		1.05
O5	2.370(6); 2.388(5); 2.485(5)						
	0.36; 0.34; 0.27						0.97
O6	2.446(6)						
	0.30					0.74	1.04
$\Sigma_A\ v^b$	2	1	1	1	1	1	

[a] Bond valence sum of all cationic contributions to each oxygen atom.
[b] Bond valence sum of all anionic contributions to each cation.

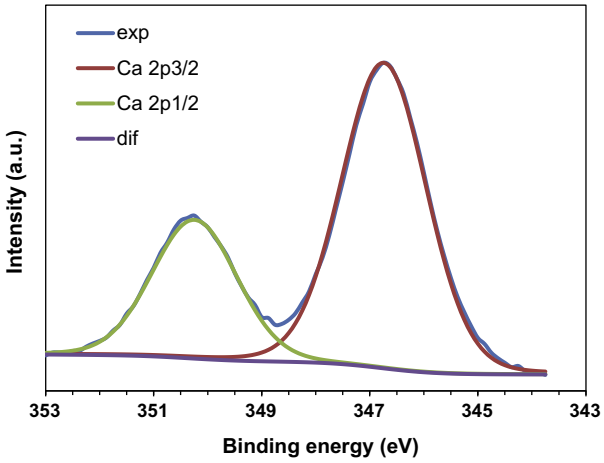

Fig. 7. XPS Ca 2p core level spectrum of calcium diglyceroxide.

indicating that the interactions between Ca^{2+} and glyceroxide ions are weaker. This finding is reasonable because the increase in coordination number (from 6 in CaO/calcite to 7 in calcium diglyceroxide) implies a Ca–O bond strength reduction.

In CaD, hydrogen bonds play a determinant role. The most probable hydrogen bonds are listed in Table 3 and visualised in Fig. 6B. There are two very strong H-bonds, one involving two O1 atoms of the same tetramer and a second involving O3 atoms belonging to neighbouring tetramers. The other H-bonds that stabilise the resulting packing of the tetramers involve the oxygen atoms O1, O2, O4 and O6 of a tetramer with the atoms O1, O4 and O3 of adjacent tetramers. Notice that O5 is not involved in the formation of H-bonds. The corresponding balance of bond valences is described in Table 2, assuming that all C–O bonds are single bonds. For calcium, bond valences were estimated from the individual Ca–O distances d_i by the expression $v_i = K_{Ca}\ d_i\ \exp(-p_{Ca}\ d_i)$, where $p_{Ca} = 3.13$ is taken from Rius and Plana [25] and Allmann [26] and K_{Ca} is fitted to the individual coordination polyhedron to satisfy the charge of Ca^{2+}. The bond valences for H atoms are listed in Table 3 and were estimated from the O···O distances derived from Fig. 5 according to Lippincott and Schroeder [27]. As observed, for each atom, the summation of the bond valences agrees well with the corresponding charge of the element.

Table 3
Probable hydrogen bonds in calcium diglyceroxide. For clarity, assumed protons have been added in parentheses. The ESDs of O···O lengths are given in parentheses. The bond valences for the O–H bonds were derived from Fig. 5 in Lippincott and Schroeder [27].

H bond	Length in Å	Bond valence in *vu*
O1–(H1)–O1	2.41(1)	0.50
O2–(H2)···O3	2.61(1)	0.75
O3–(H3)–O3	2.44(1)	0.50
O4–(H4)···O1	2.70(1)	0.79
O6–(H6)···O3	2.59(1)	0.74

As previously mentioned, the bulk structure of CaD may be explained as a collection of tetramer units held together by a system of H-bonds. Low-nuclearity Ca-based molecular systems are extremely rare [28]. The coordination of Ca^{2+} by anionic ligands, such as carboxylates, phosphonates and sulphonates, almost invariably results in coordination polymers (1D, 2D or 3D) due its variable coordination number and geometry [29,30].

On the other hand, CaD is interesting for its catalytic behaviour, which mainly depends on its surface structure. To determine the probable surface structure and the mechanism favouring catalysis, knowledge of the bulk structure will be combined with surface X-ray photoelectron measurements of the O 1s region and IR results.

Fig. 8 represents the (100) surface obtained by interrupting the crystal structure through the outwards-pointing O3 atoms, that is, by breaking the symmetrical H bonds corresponding to O3···O3 = 2.44 Å shown in the deeper layer. The strong H-bond interactions between two O3 atoms of neighbouring tetramers necessitate that only every other oxygen atom can be a –OH group, whereas the other must correspond to O^- to preserve charge neutrality. Surface characterisation by XPS (Fig. 9) yields an asymmetrical O 1s signal that can be deconvoluted into two components at 531.4 and 532.7 eV, with respective areas of 18.5% and 81.5%, which should be assigned to O^- and OH^- groups [31], respectively. These values agree well with the existence of 1 outer O^- in front of 5 outer OH^- based on the structural data (17% and 83%, respectively). Considering that the surface density of O^- sites is 0.55 sites nm^2 (assuming that (100) face is predominantly exposed), the specific surface area of CaD is 1.2 m^2/g (as determined by N_2 adsorption) and the FAME yield at 30 min. was 22%, the TOF number of CaD for FAME production has been estimated as ca. 55 s^{-1}. This value is comparatively larger than others published for CaO/Al_2O_3 catalysts at 50 °C (0.028 and 0.012 s^{-1} for 60 and 80 CaO wt.%, respectively) [32] or for $KF/MgO\text{-}La_2O_3$ catalysts at 65 °C (0.033 s^{-1}) [33]. CaD presents a much faster reaction rate than other basic catalysts; it possesses a low surface area and low basic sites surface densities; consequently, its TOF number must be quite large.

The base-catalysed transesterification mechanism for homogeneous reactions is well-established. In contrast, the mechanism

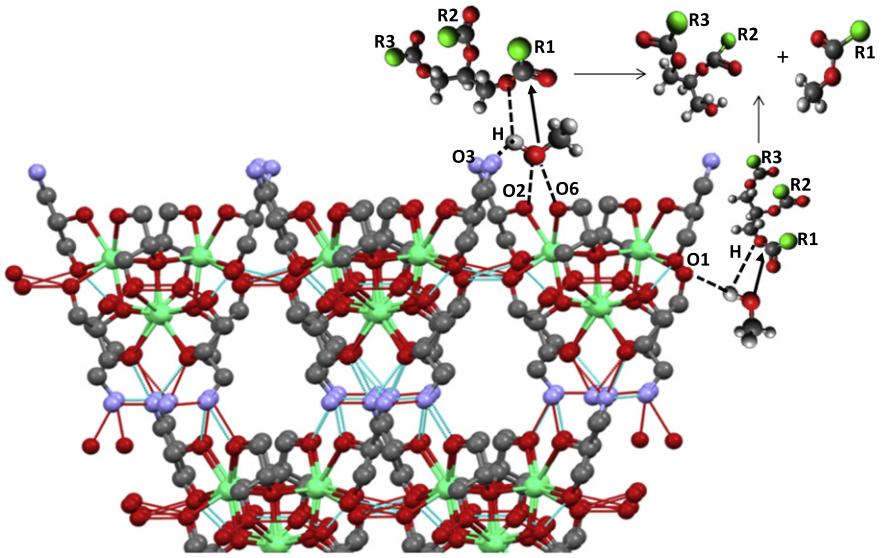

Fig. 8. Tetramer packing of calcium diglyceroxide along the (1 0 0) surface with O3 atoms in blue. The tentative transesterification mechanisms of triglyceride molecules are also given. Dot lines correspond to possible H-bond interactions. (For interpretation of the references to colour in this figure legend, the reader is referred to the web version of this article.)

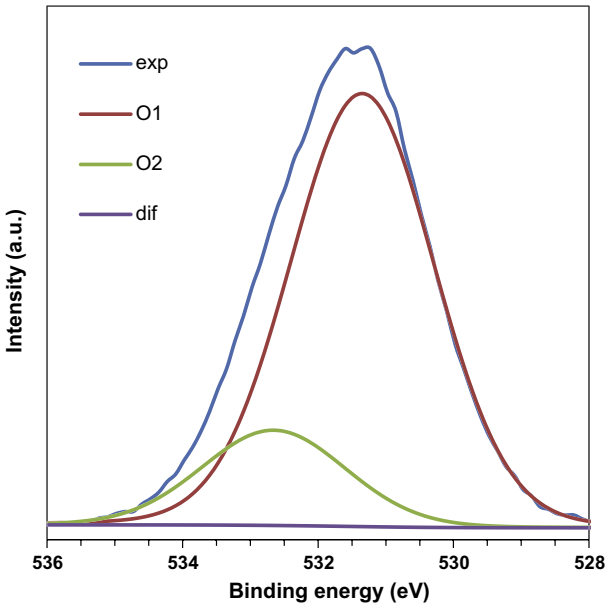

Fig. 9. XPS O 1s core level spectrum of calcium diglyceroxide.

for basic sites at the surface of solid catalysts remains controversial. Two main mechanisms have been proposed: the Langmuir–Hinselwood (LH) mechanism and Eley–Rideal (ER) mechanism [34–36]. Disregarding the exact nature of the mechanism, both have the following common features: (i) methanol is first chemisorbed and activated by surface basic sites, forming a methoxide nucleophile, and (ii) the triglyceride molecule must approach the surface to either react with the activated methoxide species (ER) or to be chemisorbed on a surface site close to that of methoxide species for subsequent reaction with it (LH). Considering these latter requirements and the surface features of CaD disclosed by the structural study, the superior catalytic activity of CaD can be explained as follows (Fig. 8). Thus, the abstraction of a proton from methanol can be accomplished by interaction of a methanol molecule with two O3 oxygen atoms belonging to adjacent tetramers. It must be remembered that only one O3 atom of the two O3 atoms of neighbouring tetramers is protonated (O3–H···O3) as consequence of the strong H-bond between them. This fact may increase the affinity of this non-protonated oxygen atom for the OH hydrogen of the methanol molecule favouring the formation of the methoxide anion. At the same time, the further release of this proton by transference to the diglyceride molecule is also favoured to preserve the electron neutrality in CaD. Moreover, the approximation of methanol molecules to the CaD surfaces would be stabilised by H-bond interactions between the oxygen atom of the methanol with the hydroxyl groups O2 and O6 or O1 and O4, depending on the surface exposed (see Fig. 8).

On the other hand, the large, very hydrophobic triglyceride molecules can approach the CaD surface because of the special orientation of the two adjacent glyceroxide units that interact with the Ca^{2+} ions through the O1 and O2 atoms and expose their lipophobic CH_x units outward. This arrangement facilitates the approach of the fatty acid units and the attack of the methoxide ions to the carbonyl groups of the approaching triglyceride molecule. The same can be applied to the formation by a sequential process of diglycerides, monoglycerides and glycerol with the consequent formation of methyl esters. Therefore, the high activity of CaD in the transesterification of triglycerides when compared to that of CaO can be explained by the particular interaction between glyceroxide and calcium ions, which creates a surface with hydrophobic and hydrophilic sites and a hydrogen bond network favouring the approaching of methanol and triglyceride molecules.

When using CaO, the methanol molecules can easily approach its polar surface, thus forming methoxide ions and decreasing the accessibility of the more hydrophobic triglycerides molecules. Once CaD is formed because of the progress of the reaction, the existence of hydrophobic and hydrophilic sites favours the methanolysis process.

4. Conclusions

We report here the structural and catalytic features of calcium diglyceroxide, $Ca(C_3H_7O_3)_2$, the active phase in biodiesel production when calcium oxide is used as a solid catalyst. Other techniques, such as Differential Thermal Analysis-Thermogravimetry (DTA-TG), Scanning Electron Microscopy (SEM) and Fourier

Transform-Infrared spectroscopy (FT-IR) spectroscopy have been employed for the full characterisation of the solid. Based on the crystallographic and characterisation data, a plausible explanation has been proposed to account for the high catalytic activity of calcium diglyceroxide relative to CaO. The crystal structure of calcium diglyceroxide is comprised of isolated tetramers, $Ca_4(C_3H_7O_3)_8$, which are held together by a complex H-bond network. When the Ca diglyceroxide crystal structure is interrupted at the surface, non-protonated O atoms are exposed. This finding has also been corroborated by X-ray Photoelectron spectroscopy (XPS) of the O 1s core level. These basic oxygen anions, absent in CaO, can easily abstract an H atom from the OH group in methanol, yielding a surface methoxide anion. The rest of the mechanism proceeds as established: the nucleophilic methoxide species attacks one of the carbonyl groups of an approaching triglyceride molecule to create the diglyceride molecule. This process occurs sequentially with the formation of monoglycerides and glycerol. Lipophilic CH_x units of the glyceroxide anions pointing away from the surface also favour the approach of the triglyceride molecule, with long lipophilic fatty acid chains, to the adsorbed methoxide species.

Acknowledgments

This investigation was partially conducted by members of the Associated Unit ICP-CSIC-UMA (“Laboratorio de Materiales para Catálisis”). The authors are grateful for financial support from the Spanish Ministry of Science and Innovation (MAT2010-15175, ENE2009-12743-C04-01 and 03, MAT2009-07967, NANOSELECT CSD2007-00041 projects), Junta de Andalucía (P09-FQM-5070) and FEDER.

References

[1] A. Grün, F. Bockisch, Ber. Dtsch. Chem. Ges. 43 (1910) 1291.
[2] T.A. Wheeler, Chem. News 142 (1931) 241.
[3] K. Fujii, W. Kondo, Z. Anorg, Allg. Chem. 359 (1968) 296.
[4] M. Di Serio, R. Tesser, L. Pengmei, E. Santacesaria, Energy Fuels 22 (2008) 207–217.
[5] M. López Granados, M.D.Z. Poves, D. Martin Alonso, R. Mariscal, F. Cabello Galisteo, R. Moreno-Tost, J. Santamaria, J.L.G. Fierro, Appl. Catal. B- Environ. 73 (2007) 317–326.
[6] M.C.G. Albuquerque, I. Jiménez-Urbistondo, J. Santamaría-González, J.M. Mérida-Robles, R. Moreno-Tost, E. Rodríguez-Castellón, A. Jiménez-López, D.C.S. Azevedo, C.L. Cavalcante Jr., P. Maireles-Torres, Appl. Catal. A 334 (2008) 35–43.
[7] J.M. Rubio-Caballero, J. Santamaría-González, J. Mérida-Robles, R. Moreno-Tost, A. Jiménez-López, P. Maireles-Torres, Appl. Catal. B 91 (2009) 339–346.
[8] M. Kouzu, T. Kasuno, M. Tajika, S. Yamanaka, J. Hidaka, Appl. Catal. A- Gen. 334 (2008) 357–365.
[9] M. Kouzu, M. Tsunomori, S. Yamanaka, J. Hidaka, Adv. Powder Technol. 21 (2010) 488–494.
[10] M. López Granados, A.C. Alba-Rubio, F. Vila, D. Martín Alonso, R. Mariscal, J. Catal. 276 (2010) 229–236.
[11] M. López Granados, D. Martín Alonso, I. Sádaba, R. Mariscal, P. Ocón, Appl. Catal. B- Environ. 89 (2009) 265–272.
[12] E. Mendelovici, R.L. Frost, T. Kloprogge, J. Raman Spectrosc. 31 (2000) 1121–1126.
[13] A. Mudalige, J.E. Pemberton, Vib. Spectrosc. 45 (2007) 27–35.
[14] A.A. Davydov, M.L. Shepotko, A.A. Budneva, Kinet. Catal. 35 (1994) 272–278.
[15] P. Kabner, M. Baerns, Appl. Catal. A- Gen. 139 (1996) 107–129.
[16] K. Chandran, R. Nithya, K. Sankaran, A. Gopalan, V. Ganesan, B. Mater. Sci. 29 (2006) 173–179.
[17] A. Boultif, D. Louer, J. Appl. Cryst. 37 (2004) 724–731.
[18] O. Vallcorba, J. Rius, C. Frontera, I. Peral, C. Miravitlles, J. Appl. Cryst. 45 (2012) 844–848.
[19] J. Rius, Acta Cryst. Section A 67 (2011) 63–67.
[20] H.M. Rietveld, J. Appl. Cryst. 2 (1969) 65–71.
[21] B.H. Toby, J. Appl. Cryst. 34 (2001) 210–221.
[22] A.C. Larson, R.B. von Dreele, Los Alamos National Laboratory, Report No. LA-UR-86-748, 2000.
[23] H. Van Doveren, J.A.Th. Verhoeven, J. Electron Spectrosc. Relat. Phenom. 21 (1980). 265–.
[24] A.B. Christie, J. Lee, I. Sutherland, J.M. Walls, Appl. Surf. Sci. 15 (1983) 224.
[25] J. Rius, F. Plana, Anal. Química 80B (1982) 147–149.
[26] R. Allmann, Monatsh. Chem. 106 (1975) 779–793.
[27] E.R. Lippincott, R. Schroeder, J. Chem. Phys. 23 (1955) 1099–1106.
[28] K.D. Demadis, M. Papadaki, I. Císarova, Appl. Mater. Interfaces 2 (2010) 1814–1816.
[29] R.M.P. Colodrero, A. Cabeza, P. Olivera-Pastor, M. Papadaki, J. Rius, D. Choquesillo-Lazarte, J.M. García-Ruiz, K.D. Demadis, M.A.G. Aranda, Cryst. Growth Des. 11 (2011) 1713–1722.
[30] A.E. Platero Prats, V.A. de la Peña-O'Shea, M. Iglesias, N. Snejko, A. Monge, E. Gutiérrez-Puebla, ChemCatChem 2 (2010) 147–149.
[31] J.F. Moulder, W.F. Stickle, P.E. Sobol, K.D. Bomben, Handbook of X-ray Photoelectron Spectroscopy, Perkin-Elmer Corporation, Minnesota, 1992.
[32] E.S. Umdu, E. Seker, Biores. Technol. 106 (2012) 178–181.
[33] R. Song, D. Tong, J. Tiang, C. Hu, Energy Fuels 25 (2011) 1686–2679.
[34] T.F. Dossin, M.F. Reyniers, R.J. Berger, G.B. Marin, Appl. Catal. B: Environ. 61 (2006) 35–45.
[35] X. Liu, H. He, Y. Wang, S. Zhu, X. Piao, Fuel 87 (2008) 216–221.
[36] A. Chantrasa, N. Phlernjai, J.G. Goodwin Jr., Chem. Eng. J. 168 (2011) 333–340.